Performance of Neutron Detectors for JLab Experiment E93–026

T. Eden

Thomas Jefferson National Accelerator Facility
12000 Jefferson Ave.
Newport News, VA 23606

Abstract

A report on the performance of large–volume plastic–scintillator detectors for neutrons is presented. The neutron detectors will be used in JLab experiment E93–026 [1]; which will measure the asymmetry of neutrons from the quasielastic $\vec{d}(\vec{e}, e'n)p$ reaction at four different squared four–momentum transfers (Q^2). Measurements of the spin–dependent neutron asymmetry from this reaction yields information about the charge structure of the neutron; namely, the Sach's elastic electromagnetic form factor G_E^n of the neutron. From this study, the average observed intrinsic time resolution for 79 neutron bars was less than 200 ps and the position resolution was 55 mm full width at half maximum.

1 Introduction

To achieve reasonable energy resolutions to separate neutrons which emanate from elastic events to those from inelastic processes (*i.e.*, Δ excitations), it is important to understand the intrinsic time dispersion of the neutron counters that will be used in the experiment. In JLab experiment E93–026, neutrons will be measured via the *time–of–flight* method. The question then, is at what flight path can we place the neutron detector to discriminate between neutrons that come from different processes without sacrificing much in the way of solid angle (*e.g.*, count rate). To answer this question, we must examine the intrinsic time dispersions of these neutron counters.

The fractional energy resolution $\Delta T/T$ of detected neutrons is given by

$$\frac{\Delta T}{T} = \gamma(\gamma+1)\left[\left(\frac{\Delta x}{x}\right)^2 + \left(\frac{\Delta t}{t}\right)^2\right]^{1/2} \tag{1}$$

Here γ is the Lorentz contraction factor [*viz.*, $\gamma = (1-\beta^2)^{-1/2}$], where β is the neutron velocity v in units of the speed of light c, Δx is the uncertainty in the neutron flight path x due to the finite thickness of the detector, and Δt is a quadrature combination of the intrinsic time dispersion of

the detector and the time dispersion introduced by the reference time signal. Eq. (1) does not include contributions to $\Delta T/T$ from the energy spread in the accelerator beam and the energy loss of the accelerator beam as it moves through the target. Although these two factors can contribute to $\Delta T/T$, they are negligible for this particular analysis. Note that the Gaussian quadrature implicit in Eq. (1), is correct only if the relative uncertainties Δt and Δx have Gaussian distributions.

One can reexpress Eq. (1) in the following form

$$\frac{\Delta T}{T} = \gamma(\gamma+1)\left(\frac{v}{x}\right)\left[\left(\frac{\Delta x}{v}\right)^2 + (\Delta t)^2\right]^{1/2} \quad . \tag{2}$$

When Δx and Δt are held fixed, the energy resolution improves linearly with an increase in flight path. For JLab E93–026, we have a similar situation to assess. Equation (2) can finally be expressed as

$$\frac{\Delta T}{T} = \gamma(\gamma+1)\left(\frac{v}{x}\right)(\Delta t)^* \ , \tag{3}$$

where $(\Delta t)^*$ is the overall time dispersion resulting from the convolution of all contributing sources; furthermore, the factor $(\Delta t)^*$ corresponds to the observed time width of a peak in a time–of–flight spectrum. For JLab E93–026, the term $(\Delta t)^*$ will represent the time difference between the electron and neutron arms.

2 Detector Configuration

The scintillators that will be used in JLab E93–026 measure 160–cm long × 10–cm high × 10–cm wide. At each end of the 160–cm length, a tapered acrylic light pipe is coupled to a Philips XP2262 photomultiplier tube (PMT). The light pipe measures 6.8 cm in length. A 2.2–cm cylindrical piece of acrylic connects the light pipe to the PMT. The anode signal from each PMT is fed into a linear fan–out module and then to a leading–edge timing discriminator. A discussion of the electronics will occur in a later section.

The detector is long in one dimension because mean timing is employed, which is based on the fact that the average of photon transit times in a long scintillator is independent of the interaction in the detector volume. A nice discussion on the mean–time technique for long scintillators can be found in Madey *et al.* [2]. In the next section, I will discuss how I employed the mean–time technique for calibrating these neutron counters.

3 Intrinsic Time Resolution (ITR)

These mean–timed detectors have inherent ITRs which include contributions from both light collection and electronics. Light collection depends on the geometry of the detector system (*i.e.*, light–pipe geometry, leading to the PMT, plays a major role). Contributions to the timing dispersion from the electronics comes from PMTs and leading–edge discriminators.

3.1 Procedure

I use energetic cosmic–ray muons as particles to generate events in the detectors. In Figs. 1 (a and b), an illustration of the ITR setup is shown. Four detectors are shown: Two identical neutron bars are placed one on top of another with a separation distance of 4.13 cm. Two ΔE paddles ($E1$ and $E2$), placed above and below the neutron bars, are used for collimating the muons through the 10 cm thickness of the neutron counter, which is predominantly the thickness a neutron will see on average. The PMTs on each detector were gain matched using a ^{228}Th gamma source (E_γ = 2.61 MeV). A 170 mV signal from the Compton peak of the 2.61 MeV gamma ray was achieved by placing the source at the center of the scintillator and adjusting accordingly each PMT high voltage (Please see Knox and Miller[3] for a complete discussion). Figure 2 illustrates the electronic logic for these tests. When there is a coincidence event between the two ΔE paddles and the two neutron bars, a 100 ns gate is generated that enables the registering of the four linear (ADC) and four logic (TDC) signals of the neutron bars by CAMAC. These signals are then recorded and stored in a raw–data file by a PC–based data–acquisition system.

In software, the raw data is processed. The mean–timed signals for the neutron bars are generated in the following way: Let the timing signals from the top and bottom detectors be t_r^{top}, t_ℓ^{top} for the top and t_r^{bot}, t_ℓ^{bot} for the bottom. The mean times are then

$$\bar{t}_{top} = \frac{1}{2}\left(t_r^{top} + t_\ell^{top}\right) \quad \text{and} \quad \bar{t}_{bot} = \frac{1}{2}\left(t_r^{bot} + t_\ell^{bot}\right) \ , \tag{4}$$

where r and ℓ denote right and left, respectively. The time difference

$$\Delta t = \bar{t}_{top} - \bar{t}_{bot} \ , \tag{5}$$

is the coincidence time between the two detectors. To unfold the single detector contribution to the coincidence signal, I use the following relation

$$\Delta t^2 = \Delta t_{top}^2 + \Delta t_{bot}^2 \ , \tag{6}$$

where Δt_{top}^2 and Δt_{bot}^2 are the individual time dispersions for the top and bottom detectors, respectively. Equation (6) is valid because I assume that two detectors of the same geometry contribute equally and in quadrature to Δt; therefore, $\Delta t_{top(bot)} = \Delta t/\sqrt{2}$. Shown in Fig. 3 is a typical coincidence time spectrum after corrections for low–ADC value TDC walk were applied.

3.2 TDC Walk

For E93–026, the method for deriving a timing logic signal will be by leading–edge triggering; and we will use CAMAC leading–edge discriminators (model 4413) to perform this task. This method is inherently subject to problems of *walk* (*i.e.*, signals with different amplitudes cross the discriminator threshold at different times). During the experiment, it will be optimum to work with as low a discriminator threshold as possible (minimize walk); however, during the experiment, we expect TDC walk for low ADC values to be present. To mimic this effect during our ITR tests, an offset arrangement of the ΔE paddles is employed (see Fig. 1c). The offset arrangement allows for muons to traverse small path lengths in the neutron–detector medium.

Small path lengths result in small ADC values; and in turn, result in TDC walk. Shown in Fig. 4 are ADC spectra with two different arrangements of the ΔE paddles: 1) Without any offset; and 2) A 2.86 cm offset.

Let me mention that by not using the ΔE paddles, small path length interactions are very prominent. A low–energy spike in the ADC spectrum is seen, which produces tails in the coincidence TDC that extend out to ~ 5 ns on both sides of the peak! Because neutrons from the target will not have such great variations in direction during the experiment, the collimating ΔE detectors provide a more realistic treatment for studying these neutron detectors using energetic muons. Low–energy walk will be present, but not with such frequency.

Figure 5 depicts the *walk* phenomenon for the two setups as described in Fig. 4. What is shown is the coincidence TDC spectrum against the ADC spectrum. For small ADC values, it is evident that TDC events begin to diverge from the mean (channel location) of the coincidence TDC peak in each arrangement. For the purpose of these tests, the offset arrangement for the ΔE paddles was chosen because there was a reasonable amount of low–energy events present. By choosing this arrangement, a correction to the coincidence TDC spectrum could be employed, without any low–energy cuts to the detector ADC spectrum. Shown in Fig. 6 is a raw coincidence TDC spectrum (top panel), and that same coincidence TDC spectrum (bottom panel) corrected for TDC walk.

The walk correction begins with a fit to the diverging part of the coincidence TDC/ADC spectrum. Shown in Fig. 7 is a typical fit with an n^{th}–order polynomial (best fits have been performed with polynomials between order five and seven). The square points shown, represent a line through the locust of points, converging to the mean of the TDC distribution, going from left to right, respectively. The line through the square points represents the fit, where the fitted function becomes the "walk" correction for those TDC events. Again, with this correction, I can reduce the effect of TDC smearing from low–energy events in the detector. Displayed in Fig. 8 is the effect the walk correction has on the two-dimensional TDC vs. ADC spectrum that was shown in Fig. 5 — the diverging signal is now corrected or "in–line" with the rest of the distribution. The amount of correction from these low–energy ADC signals for the bottom right PMT is shown in the bottom panel of Fig. 8.

3.3 Small Path Length Equals Small ADC Value?

In Fig. 4, certain arrangements of the veto counters give different distributions for the low–energy part of the ADC spectrum. The question is, what causes this behavior? First we must understand the ADC spectra for one detector. Shown in Fig. 9 is the right ADC, left ADC, and the right versus left ADC spectra for the bottom detector. One notices that the ADC spectrum for both ends of the detector are quite similar. Each spectrum has a low–energy plateau, followed by a prominent peak which corresponds to the most probable energy deposited in 10 cm of scintillator by energetic muons [4]. The spectrum depicting right versus left shows a definite band of correlation: If one tube sees a specific voltage, the other tube sees the same voltage that is within a range determined mostly by attenuation of the light within the scintillator.

Because a two–detector setup for these ITR tests is utilized, a further test can be administered to confirm that the low–energy part of ADC spectrum is geometry dependent. Shown in the bottom right panel in Fig. 9, is a two–dimensional spectra illustrating the behavior of the right PMTs for the bottom and top detectors, respectively. The correlation that is seen for one

T (MeV)	x (m)	v/x (ps^{-1})	$\Delta x/v$ (ps)	Δt^* (ps)	ΔT (MeV)
267.0	3.4	55	266	354	$\pm$ 15.4
533.0	3.4	68	216	319	$\pm$ 46.5
799.0	5.5	46	198	307	$\pm$ 59.4
1065.0	8.0	33	189	301	$\pm$ 71.1

Table 1: Fractional energy resolution ΔT for neutrons at the four different central neutron kinetic energies specified by E93–026. The time resolution in Eq. (2), $\Delta t = 235$ ps, is obtained by adding in quadrature $\Delta t_{neut} = 195.5$ ps and $\Delta t_{HMS} = 130$ ps. The values for Δt^* (column five) represent the expected coincidence time resolutions (σ) for each experimental point.

detector has mostly vanished for the two detectors. In other words, if one detector has a small–energy deposit, the other detector may see any energy deposited in its scintillator; confirming the geometrical dependence of the setup when performing these ITR tests.

4 ITR Test Results

Shown in Fig. 10 is a fit to the coincidence TDC spectrum. A normal three–parameter gaussian is used to fit the spectrum. The standard deviation of the fit is (5.53 ± 0.04) ch. By using the resolution slope of the CAMAC TDC (50 ps/ch), one can extract the coincidence time resolution; namely, (276.5 ± 2.0) ps. Extracting the single–detector contribution to the coincidence peak follows from Eq. (6); hence, $\Delta t_{top} = \Delta t_{bot} = 195.5$ ps. The average time resolution for the entire lot of neutron bars is 195.5 ps. Using this resolution, together with the time dispersion of electrons through the HMS, the expected fractional energy resolutions for the four different neutron energies are shown in Table 1.

Shown in Fig. 11 is a distribution of ITRs for all neutron detectors that were tested. The normally distributed spectrum has a fitted mean of 195.5 ps, which happens to be the actual statistical average.

5 Position Resolution

The position resolution of the neutron detectors was determined by measuring the time difference in the photon transit times of a scintillation event to each PMT. If y denotes the position of a scintillation event in a neutron detector, then

$$y = u\,(\bar{t} - t') \quad , \tag{7}$$

where u is the propagation speed of light pulses in the detector, $\bar{t}$ is the mean time of the detector, and t' is a pulse from one of the detector PMTs. To perform such a test, I utilized the ΔE detectors to select a well–defined vertical flux of cosmic–ray muons. By placing the ΔE detectors perpendicular to the neutron bars, and tilting them on their sides, I restrict the

cosimc–ray muon measurements to a small (40–mm wide) region along the axis of the 160–cm–long detector. Shown in Fig. 12 are position spectra that were obtained with the aformentioned ΔE–paddle configuration centered at three different regions along the 160–cm length of the detector. The width of these peaks is indicative of the position resolution for these neutrons detectors, which have a fitted standard deviation of $\sim$ 3.1 ch. Shown in Fig. 13 is a plot of the actual position versus time channel number for the data in Fig. 12. The position calibration is clearly linear as indicated by the straight line. Using the fitted calibration slope of 0.75 cm/ch, the position resolution is 55 ± 4 mm full width at half maximum. The uncertainty is due to the width of the collimating ΔE detectors used to take the data.

Finally, in Fig. 14, two position spectra are shown for one of the neutron bars without the use of the ΔE paddles in the event trigger. The top panel displays the position spectrum that is similar to what we can expect in the experiment when the neutron detector is fully illuminated. The bottom panel is the conversion of the position data to information about where, along the major axis of the detector, the event took place. This position information can be used to extract the neutron scattering angle θ_n, which is important for obtaining neutron–arm kinematical quantities.

References

[1] D. Day *et al.*, JLab Experiment E93–026.

[2] R. Madey *et al.*, Nucl. Instrum. and Meth. **214**, 401 (1983).

[3] H. H. Knox and T. G. Miller, Nucl. Instrum. and Meth. **101**, 519 (1972).

[4] J. M. Paul, Nucl. Instrum. and Meth. **96**, 51 (1971).

Detector Configuration

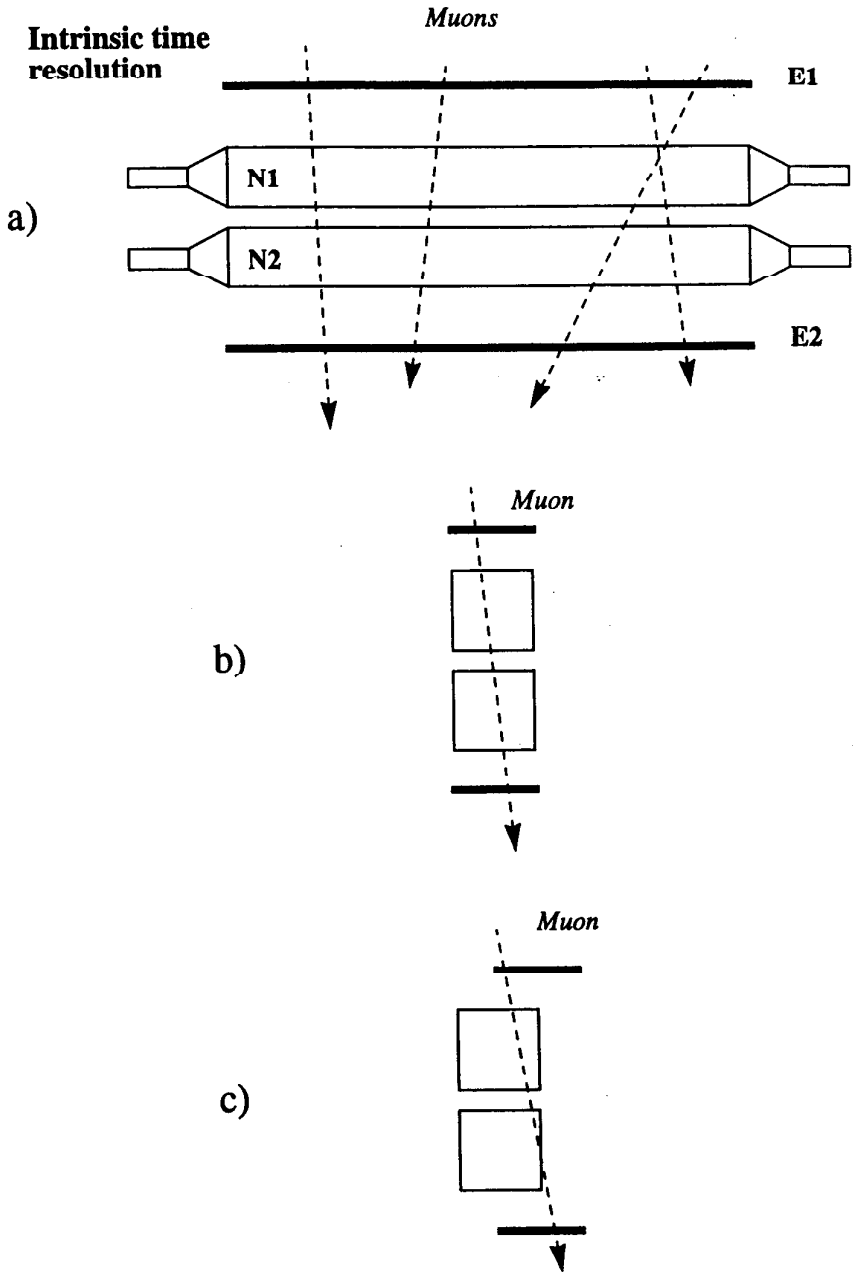

Figure 1: Detector configuration for performing intrinsic time resolution tests using energetic cosmic–ray muons: a) Side view of setup; b) End view of setup with ΔE (E1 and E2) detectors directly above and below the neutron bars; and c) Setup with offset of ΔE detectors. The offset ΔE detectors permitted acquiring small–path length events to simulate low–threshold ADC walk in the coincidence TDC spectrum.

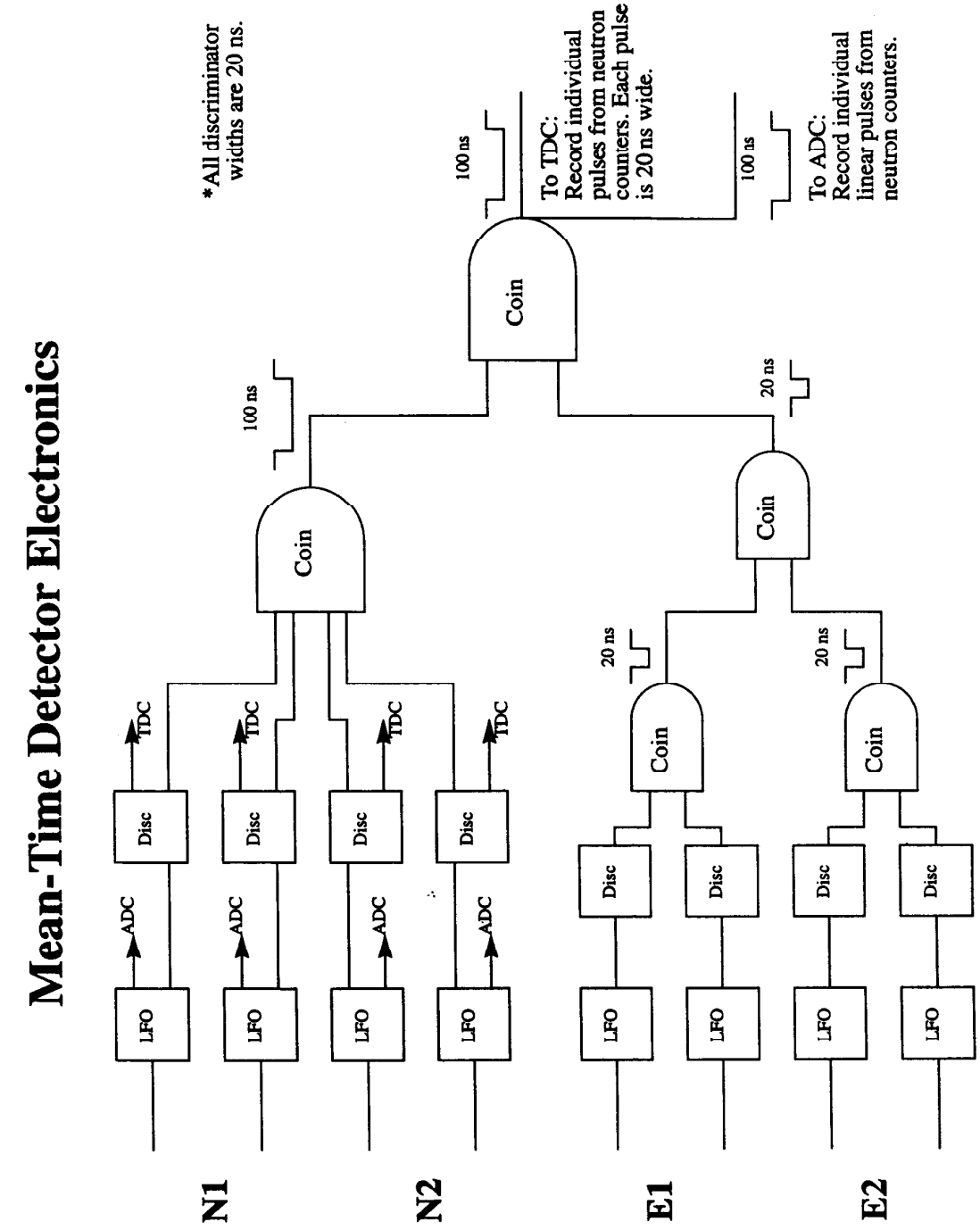

Figure 2: Electronic diagram of the neutron detector test setup.

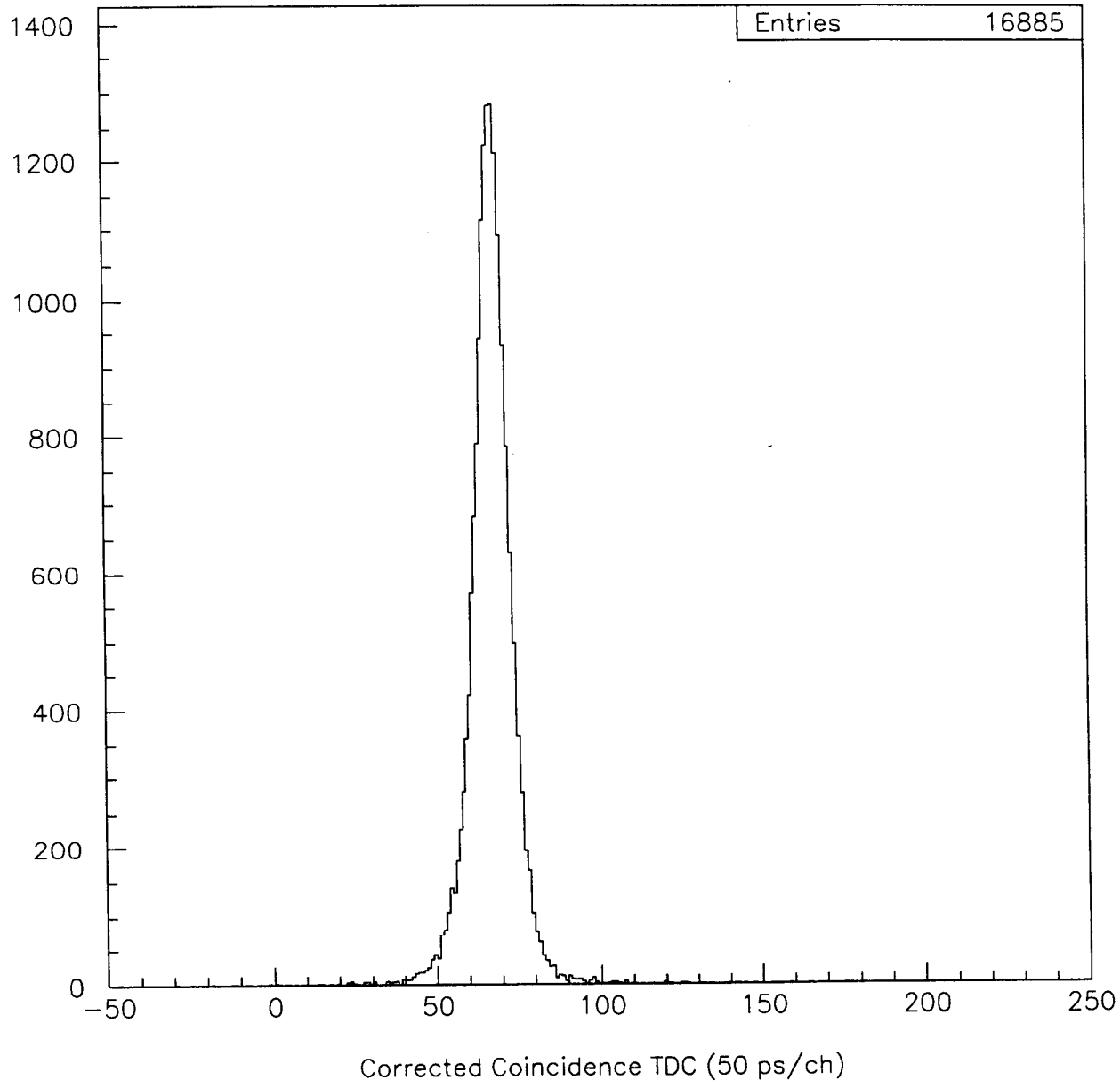

Figure 3: Typical coincidence TDC spectrum after corrections for TDC walk were applied.

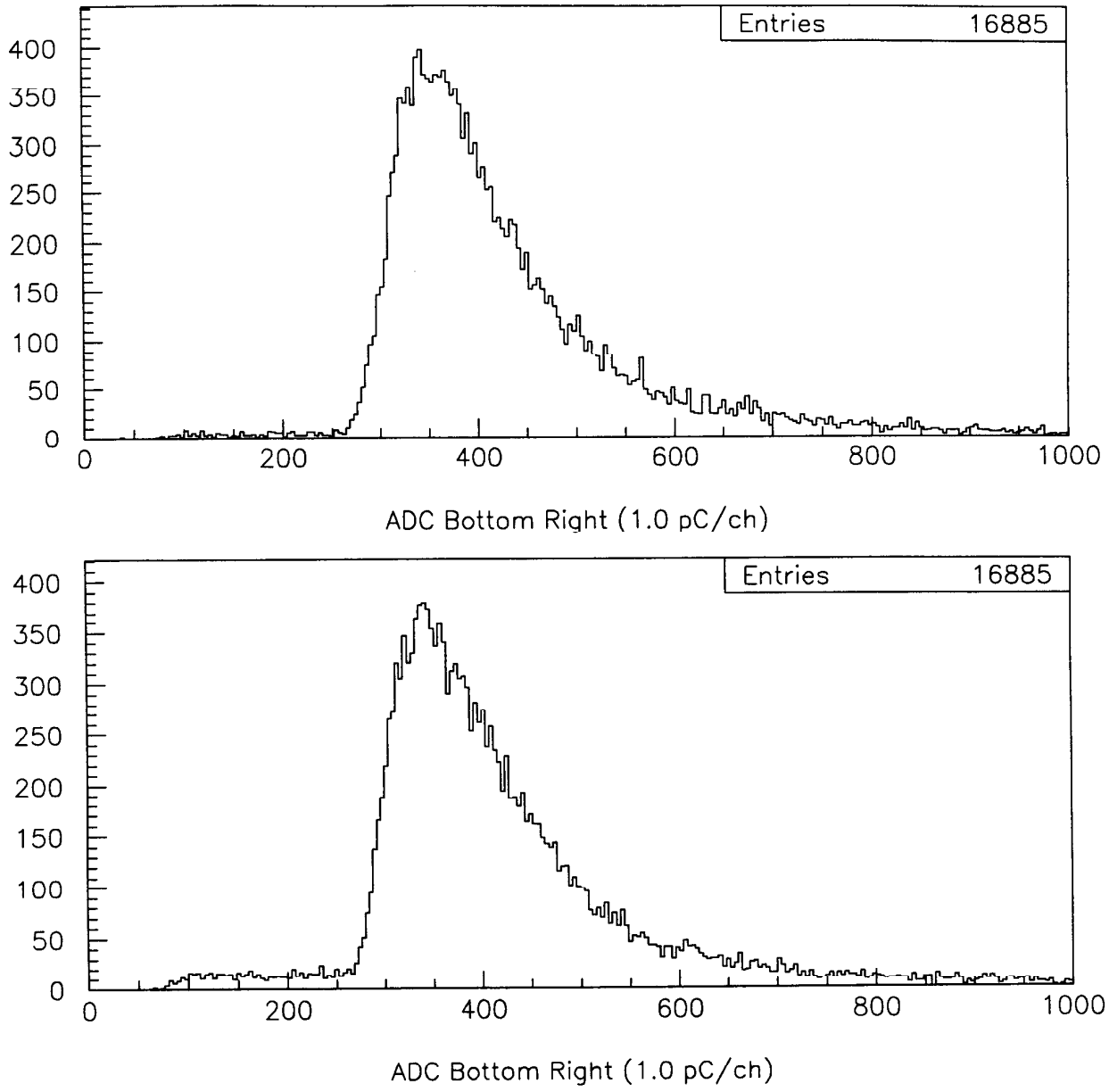

Figure 4: Top left ADC spectra for two configurations of the ΔE paddles. The top panel is without an offset to the ΔE paddles, and the bottom panel is taken with the ΔE paddles having a 2.86 cm offset. Notice the different response of the low–energy plateau when the offset of the ΔE detectors was applied.

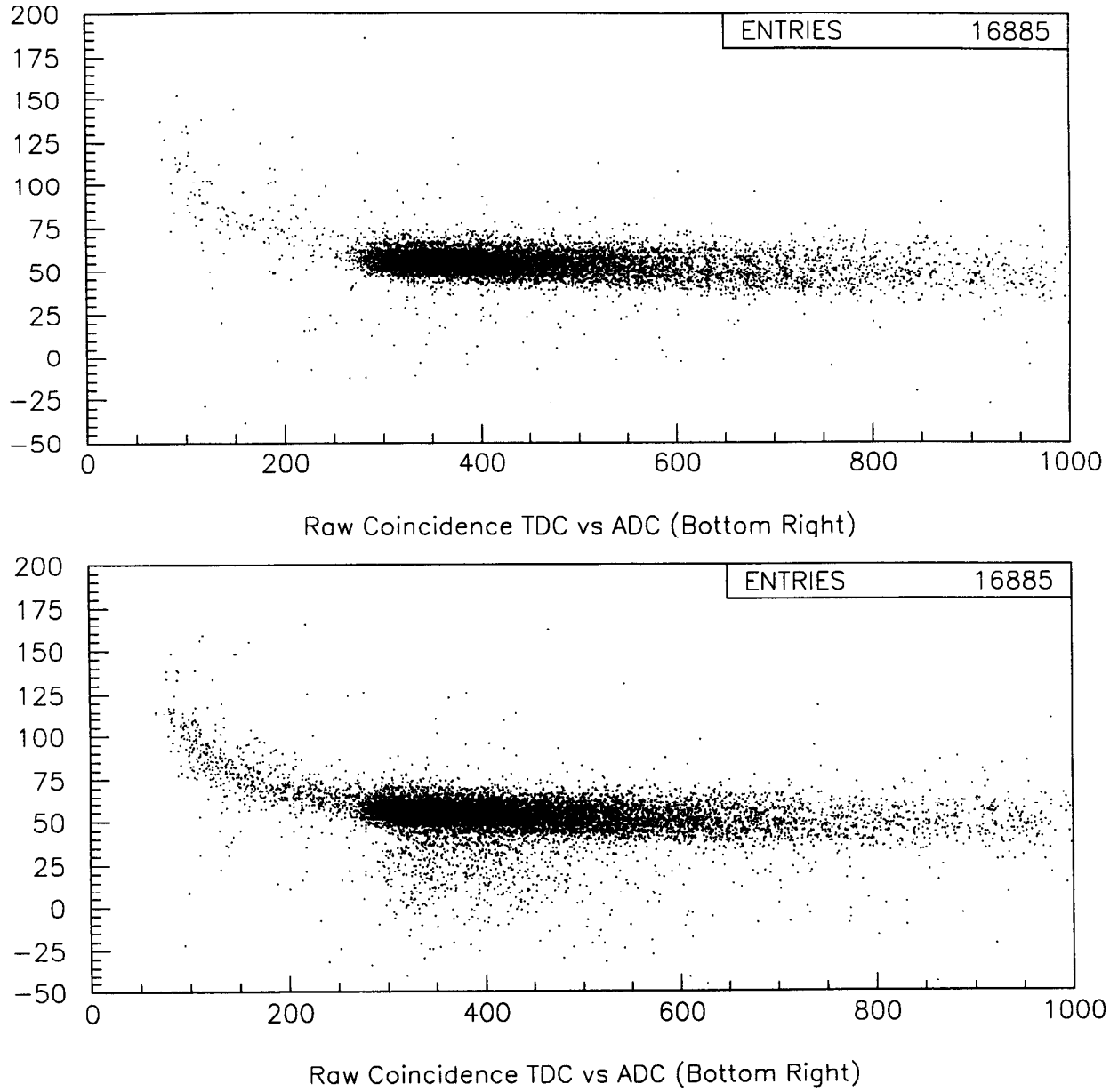

Figure 5: Two–dimensional spectra of the corrected coincidence TDC versus bottom right ADC for the two ΔE paddle configurations as described in Fig. 4. Note the correlation between low–energy ADC signals resulting in a diverging ("walk") TDC signal.

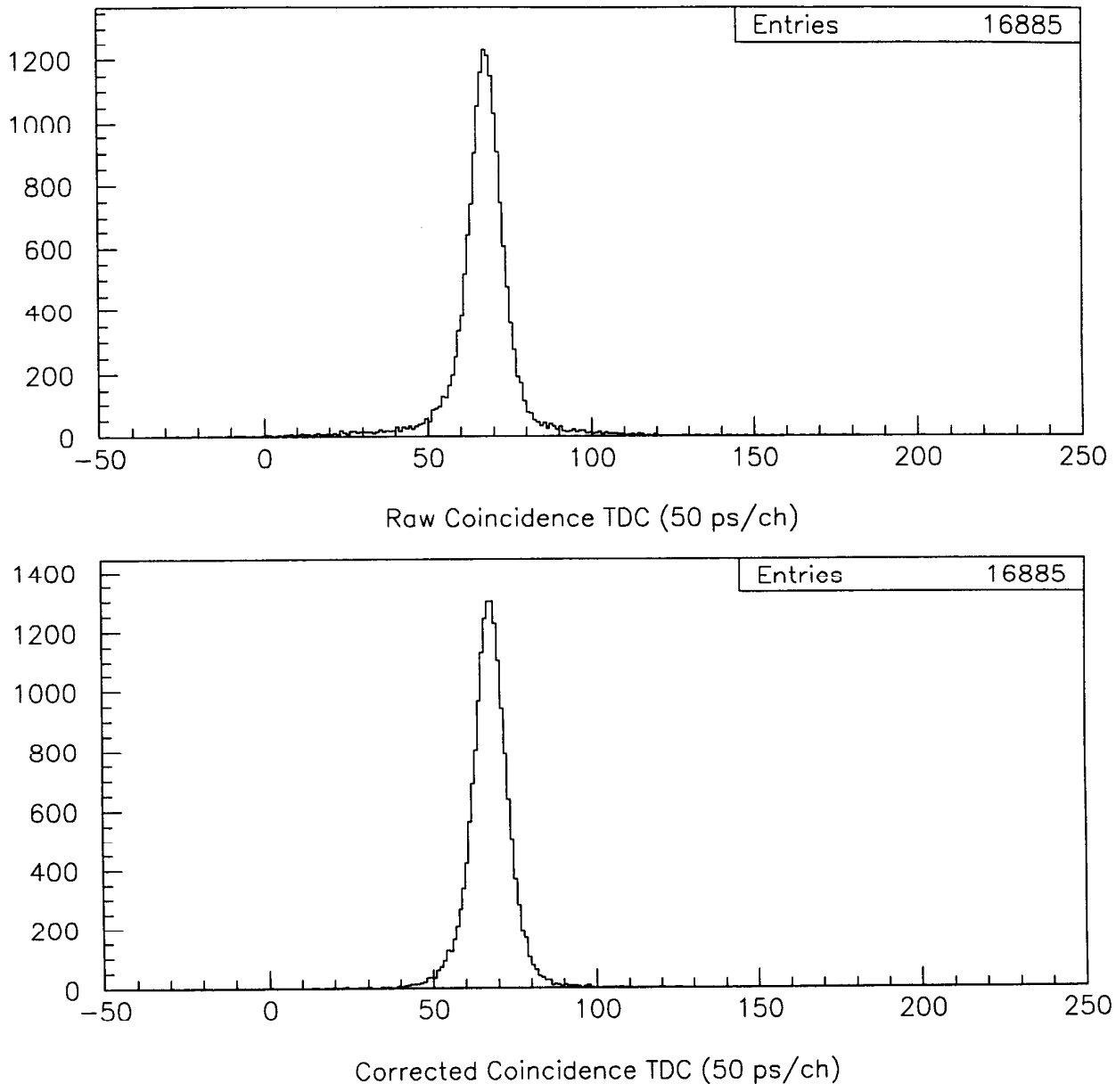

Figure 6: Shown in the top panel is a raw coincidence TDC spectrum, and in the bottom panel is the "walk" corrected coincidence TDC spectrum.

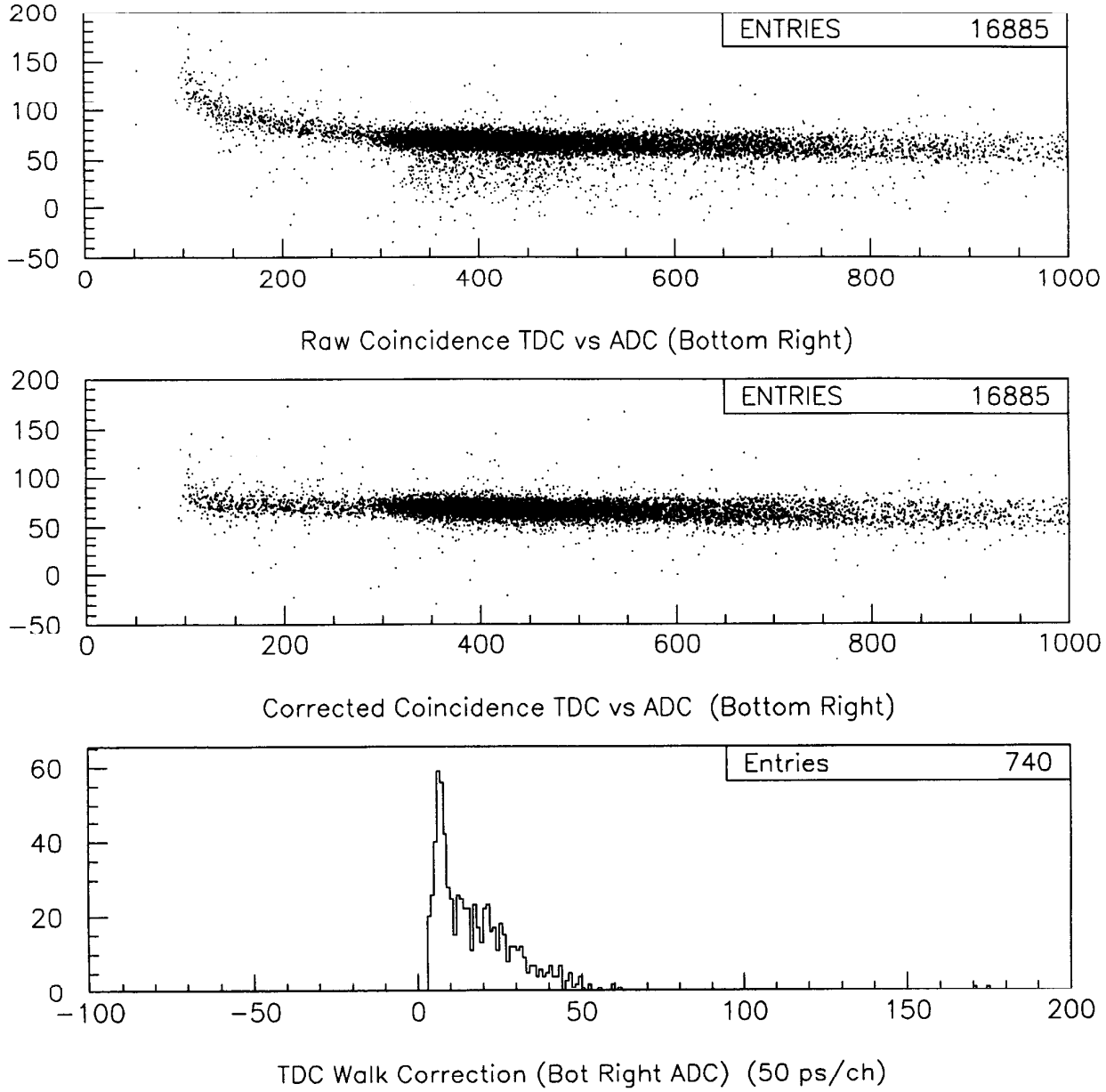

Figure 7: Two–dimensional spectra of the coincidence TDC versus bottom right ADC: Top panel is the raw spectrum; and in the middle panel is the corrected spectrum. In the bottom panel, is the contribution of "walk" corrected events from the bottom right ADC.

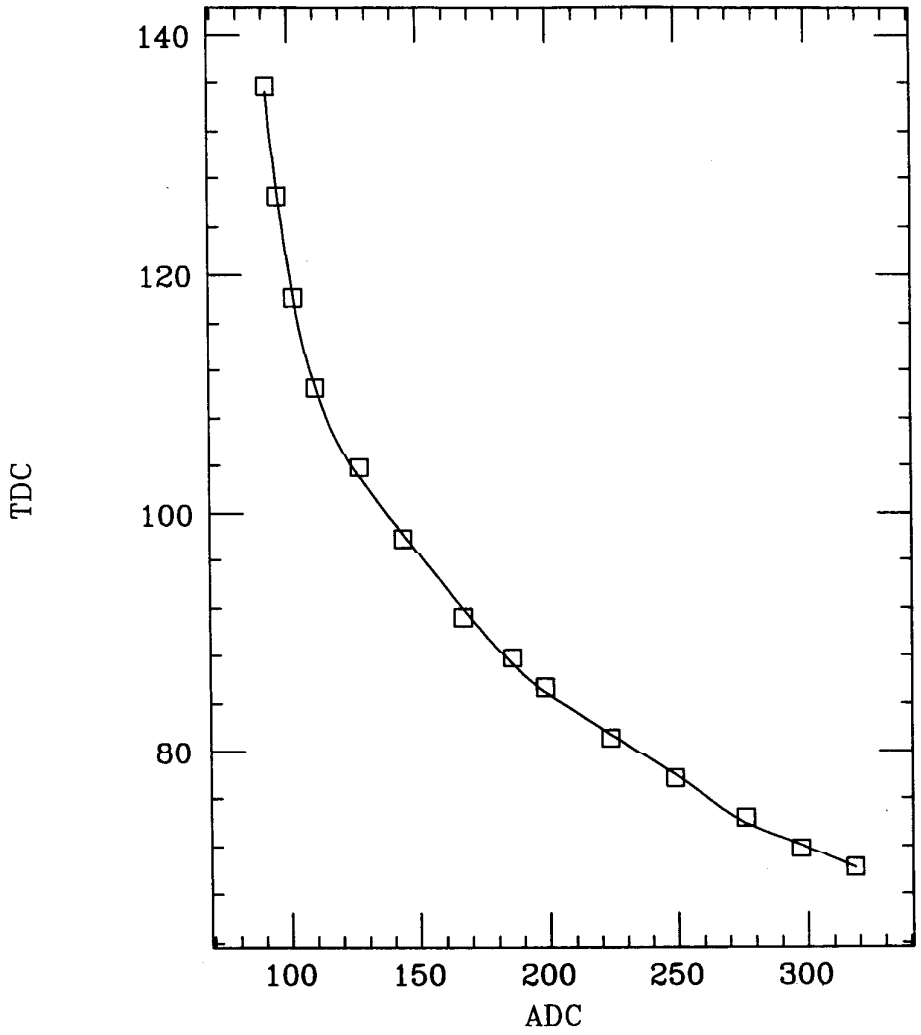

Figure 8: A fit to the two-dimensional coincidence TDC vs. ADC (bottom right) spectrum to obtain the TDC walk correction for this particular PMT. The square characters represent a line to the diverging part of the spectrum (see top panel of Fig. 7). The solid line is an n^{th} order polynomial fit through these points.

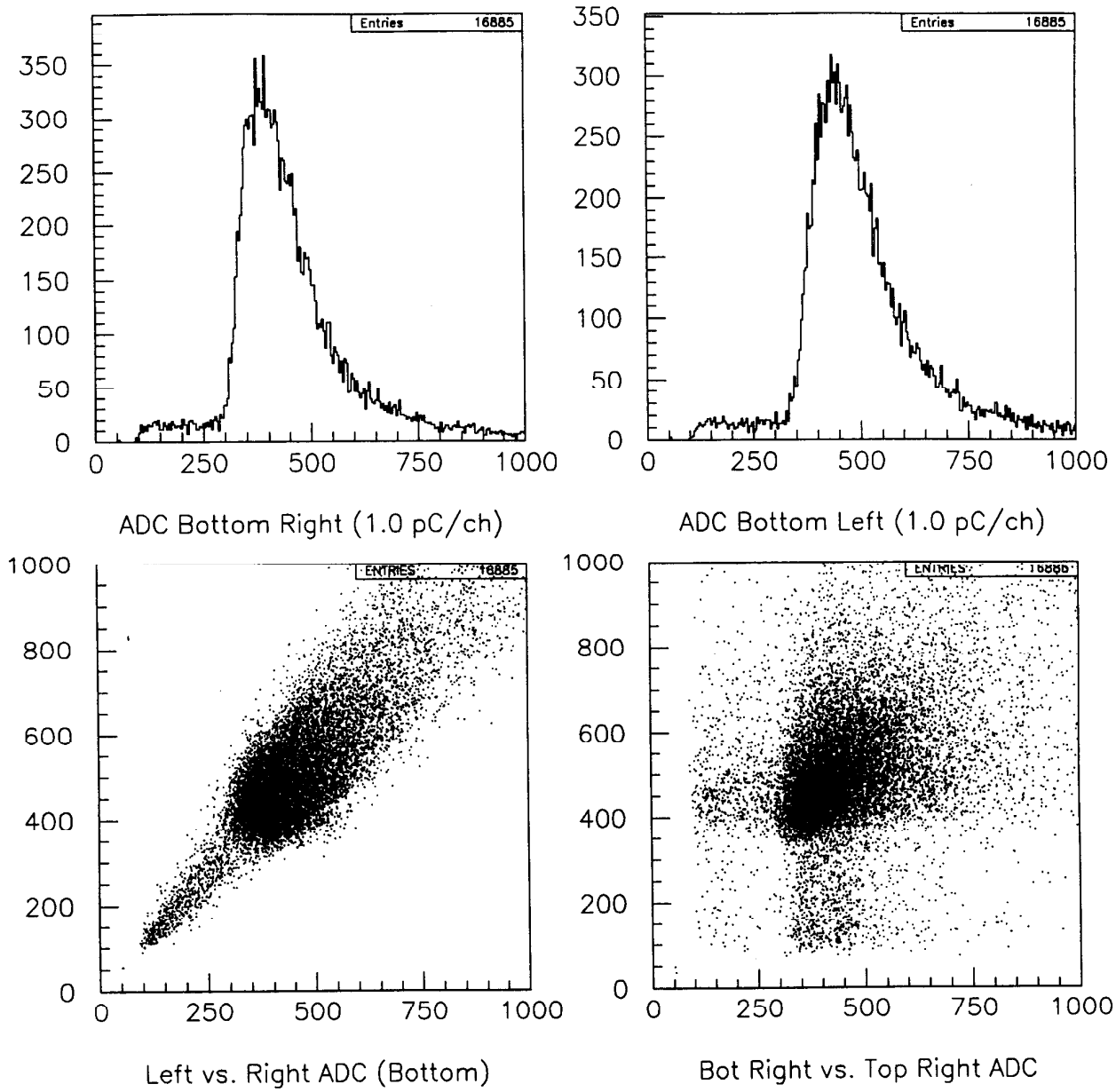

Figure 9: ADC spectra for the bottom detector. The top two panels are the individual ADC spectra for the left and right PMTs, respectively. The spectrum in the bottom left panel shows the left ADC versus right ADC for the bottom detector. Notice the strong correlation between the two signals. The spectrum in the bottom right panel shows the bottom right ADC versus the top right ADC. Notice the loss of correlation that was evident in one detector.

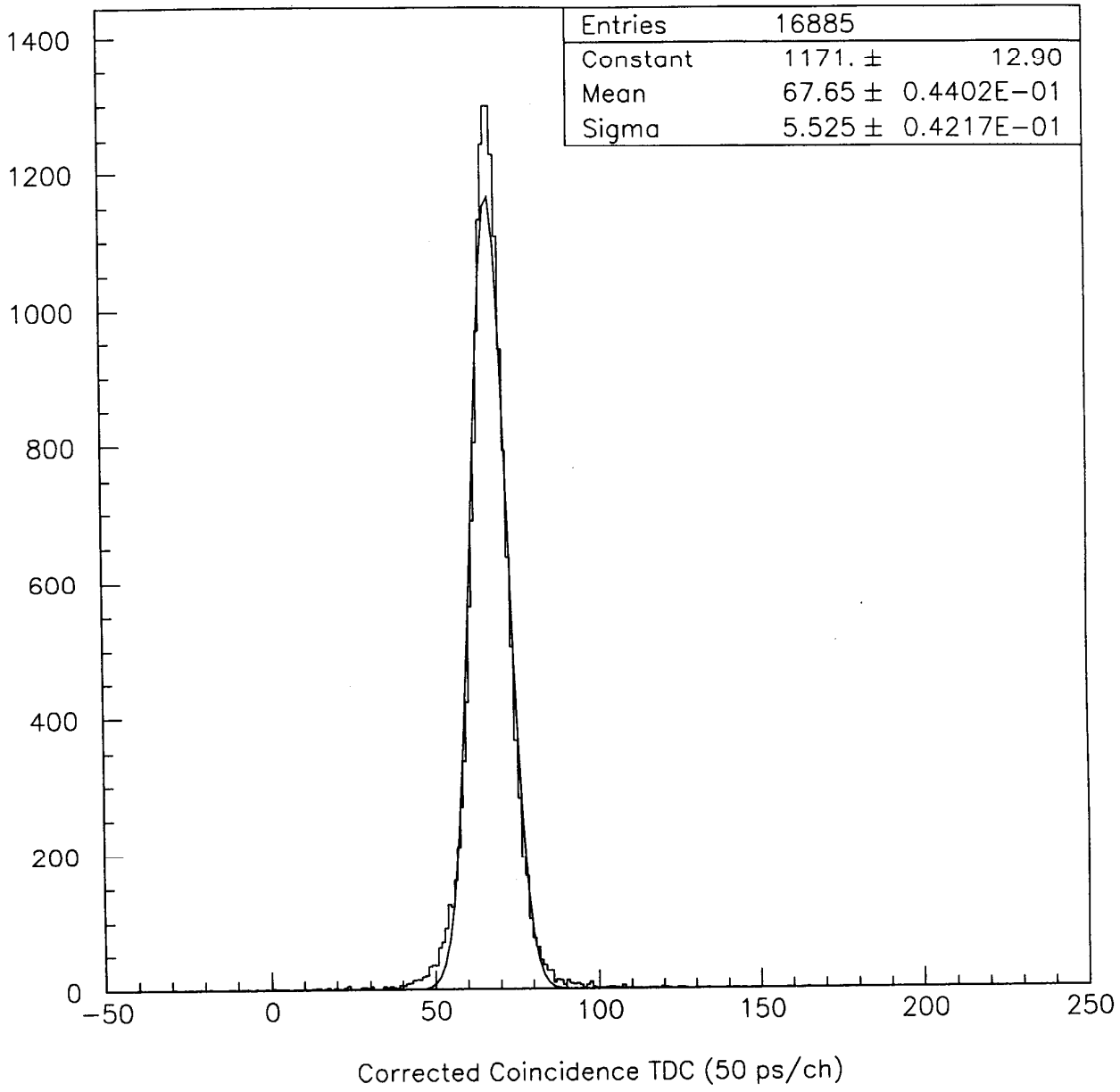

Figure 10: Typical fit to the coincidence TDC spectrum after corrections for TDC walk were applied.

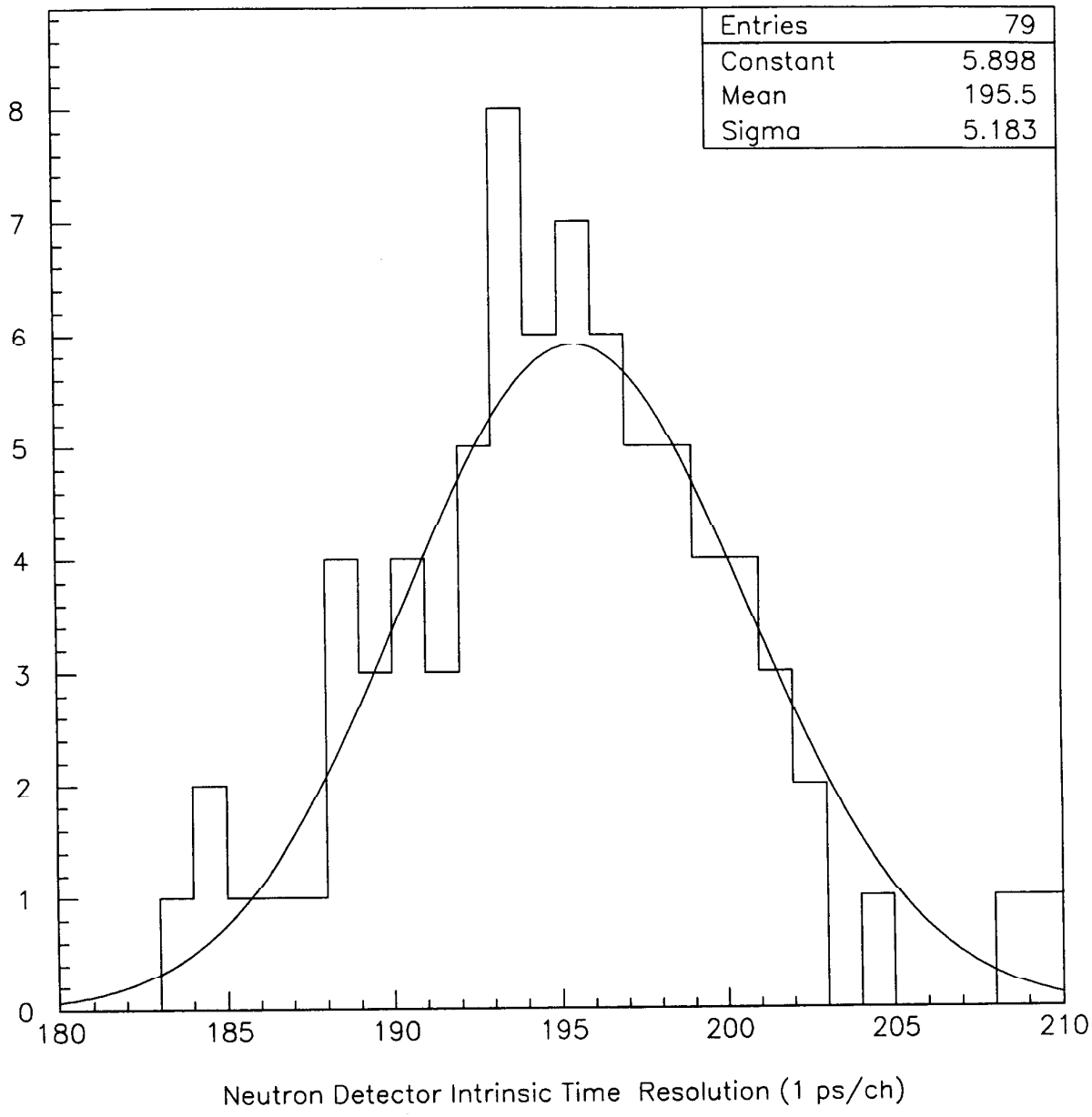

Figure 11: Distribution of intrinsic time resolutions for all neutron bars that were tested. The distribution is normal, with a fitted mean of 195.7 ps for 79 detectors.

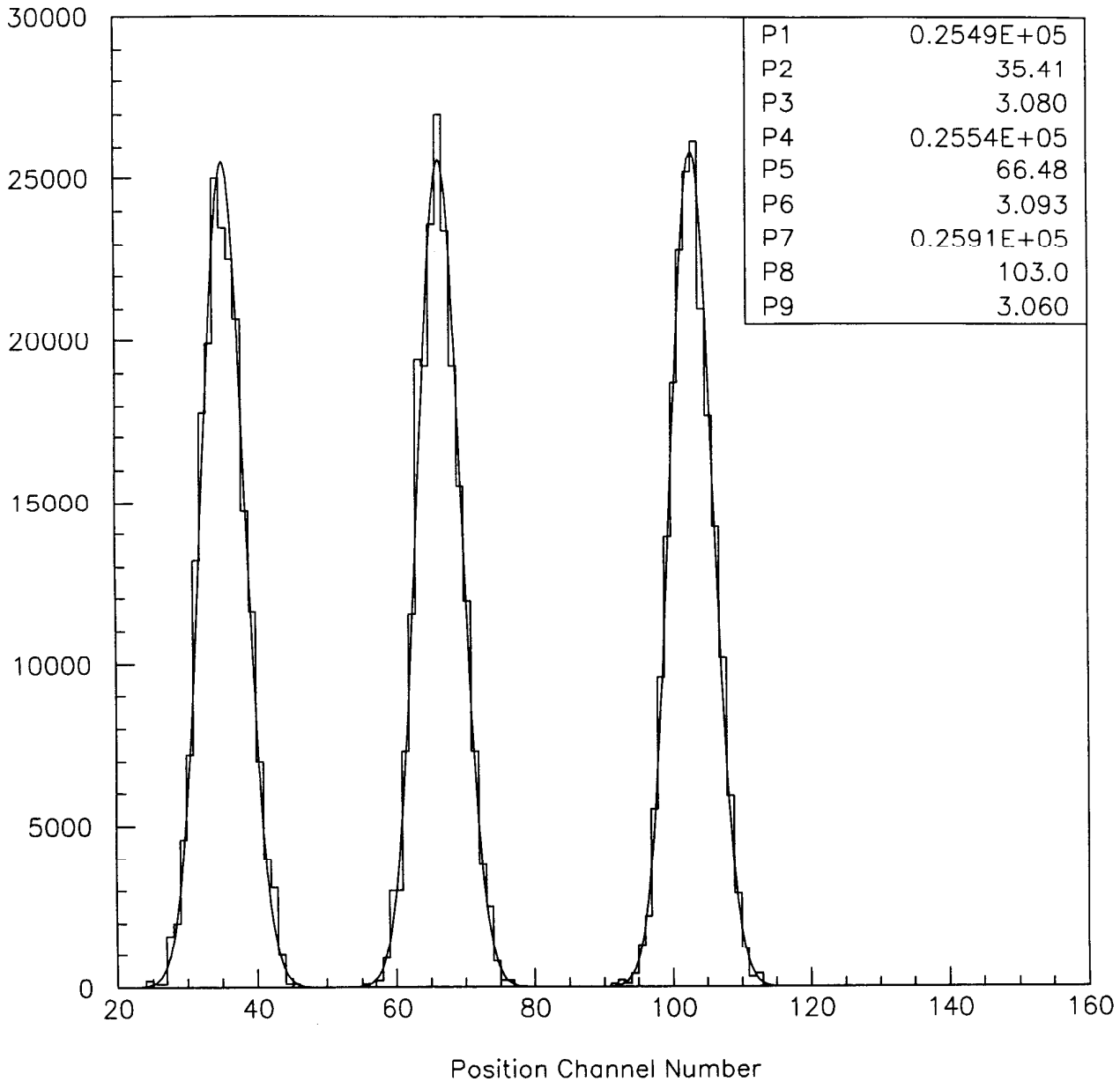

Figure 12: Position resolution measurements for three different regions of the detector using collimated cosmic–ray muons.

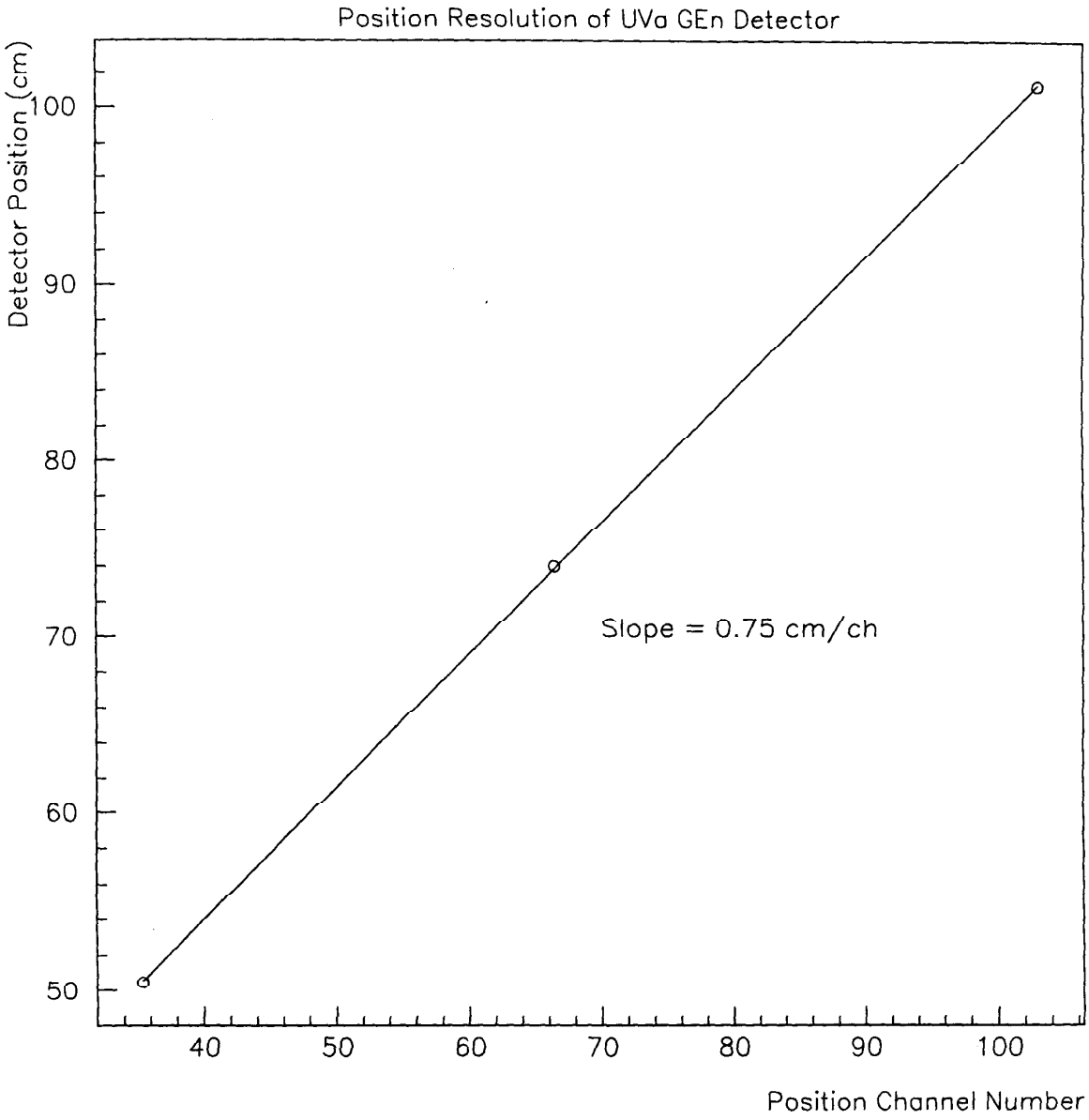

Figure 13: Plot of the actual distance versus time channel number for the data shown in Fig. 12. The linearity of the position y along the bar is given by the straight line.

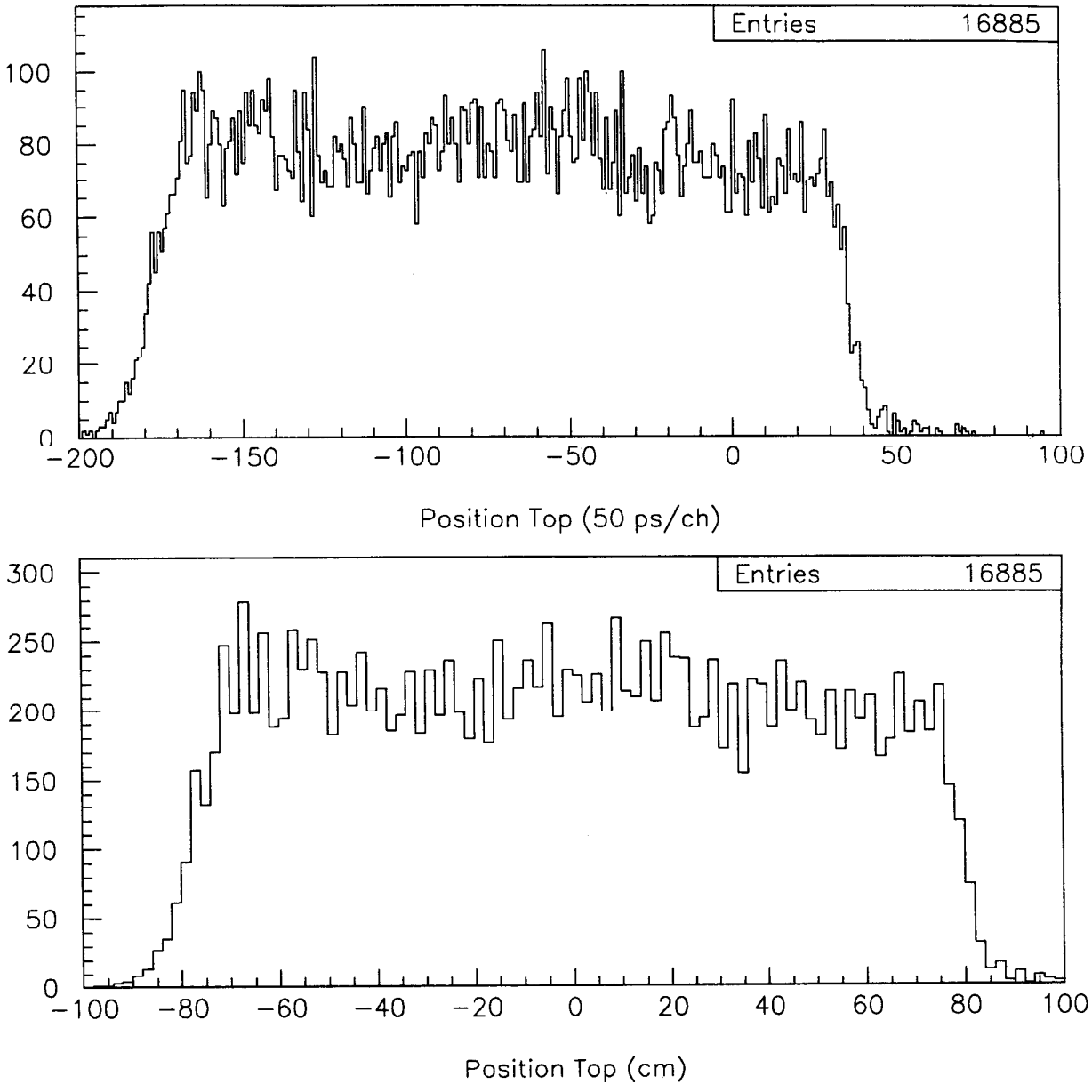

Figure 14: Position spectra of a neutron bar without using the collimating ΔE detectors in the event trigger. The top panel displays the fully illuminated neutron detector. The position spectrum is generally flat (as expected). The bottom panel shows the distribution of hits along the position–sensitive axis of the bar (± 80 cm).